

Preparation of Pomelo Peel-Based Biomass Carbon Aerogel-MnO₂ Composite Electrode and its Adsorption Performance of Rb⁺ and Cs⁺

^{1,2}Yaoqiang Hu, ²Min Guo, ²Xiushen Ye, ²Quan Li, ²Haining Liu*, ²Zhijian Wu

¹ Key Laboratory of Climate, Resources and Environment in Continental Shelf Sea and Deep Sea of Department of Education of Guangdong Province, Guangdong Ocean University, Zhanjiang, Guangdong 524088.

²Key Laboratory of Comprehensive and Highly Efficient Utilization of Salt Lake Resources, Qinghai Provincial Key Laboratory of Resources and Chemistry of Salt Lakes, Qinghai Institute of Salt Lakes, Chinese Academy of Sciences, Xining 810008, China.
yaoqiang.h@163.com*

(Received on 28th January 2021, accepted in revised form 23rd July 2021)

Summary: Electrosorption can be used for both desalination of seawater and high value element ions enrichment, which has attracted more and more attentions because of its merits of low energy consumption, no pollution and inexpensive. The research focuses on the preparation of novel electrodes and selective electrosorption properties. In this paper, biomass carbon aerogel was prepared by hydrothermal-freeze drying- carbonization method using pomelo peel as raw material. A composite electrosorption electrode was obtained using pomelo peel-based carbon aerogel (PCA) as main component. The surface morphology, crystal structure, specific surface area and functional groups were characterized by Scanning Electron Microscope (SEM), X-Ray Diffraction (XRD), Brunauer Emmett Teller (BET) and Fourier Transform Infrared Spectroscopy (FTIR). Then the effects of coexisted alkali/alkaline earth metal ions on the adsorption of Rb⁺ and Cs⁺ were studied. The pomelo peel-based carbon aerogel-manganese dioxide (PCA-MnO₂) composite electrode shows good adsorption performance on Rb⁺ and Cs⁺. When alkali and alkaline earth metal ions coexist, PCA-MnO₂ composite electrode exhibits the highest adsorption selectivity of Mg²⁺. The research content in this work broadens the source of electrosorption electrode and provides a reference for the study of competitive adsorption of alkali/alkaline earth metal ions.

Key words: Hydrothermal-freeze drying method; Biomass carbon aerogel; Electrosorption; Rb; Cs.

Introduction

As a desalination method, electrosorption is a non-membrane penetration process under atmospheric pressure to remove charged particles or ions in aqueous solution by large specific surface charged electrode [1]. It is promising to be used in the treatment of heavy metal ions such as copper and cadmium in metallurgy, mining, electroplating and other industries, because of its advantages of cost-effective, energy efficient and environmentally benign [2-5]. On the other aspect, it is also an ion enrichment technology. Trace cations are adsorbed on the electrode surface by electrosorption, and then change electrode potential to desorb ions by reversing circuit or remove voltage, so as to enrich and purify the target ion [6]. Therefore, it is of high research value to apply it to separate high value elements.

Rubidium (Rb) and cesium (Cs) are extremely active alkali metal elements with excellent photoelectric properties [7, 8]. Concentrations of rubidium and cesium in seawater are 0.12 mg/L and 2.3 nmol/L respectively, which make them difficult to extract commercially [9, 10]. However, salt lake brines in Qinghai and Tibet, China contain higher concentrations of rubidium and cesium as a valuable

liquid mineral resource [11]. Thus, electrosorption has great potential applications in enriching and separating Rb and Cs from salt lake brine.

The preparation of efficient selective electrode is a key factor in the development of electrosorption technology [12]. At present, electrosorption electrode materials are mainly conductive carbon materials, such as activated carbon, carbon aerogel, ordered mesoporous carbon, carbon nanotubes and graphene, etc [13]. These electrode materials have many advantages in absorbing large quantities of salt ions, such as good conductivity, large specific surface area and superior conductivity. However, some carbon materials suffer from poor wettability or poor mechanical stability. In order to utilize the advantages of carbon materials and other kinds of materials with large adsorption capacity and good selectivity, many different types of composite electrodes were prepared on the basis of conductive carbon material, like AC-TiO₂, carbon-polyaniline, RG-RF [14]. These additional components can enhance the electrosorption capacity by adjusting pore structure, wettability or improving the surface functional groups.

*To whom all correspondence should be addressed.

MnO₂ can be used as an inorganic adsorbent with good performance for many metal ions [15, 16]. However, it cannot be used as electrode material alone due to its poor conductivity. In this paper, a biomass carbon aerogel was prepared using pomelo peel as raw material by hydrothermal-freeze drying-high temperature carbonization. Then composite electrode was obtained after carbon aerogel, carbon black and MnO₂ being sprayed on graphite plate by polyvinylidene fluoride as adhesive, as shown in Fig. 1. The effects of electrode composition, voltage and coexisting ions on the electrosorption performance of composite electrode were comprehensively studied with Rb and Cs as target ions.

Experimental

Chemicals

RbCl (99.5%) and CsCl (99.5%) were provided by Xinjiang Nonferrous Metal Research Institute. MnO₂ was purchased from Tianjin Guangfu Fine Chemical Research Institute. Carbon black (cabot Vulcan xc-72), *N,N*-dimethylacetamide (99%) and polyvinylidene fluoride (99%) were purchased from Shanghai Macklin Biochemical Co. Ltd. All reagents were directly used without further purification.

Preparation of PCA and PCA-MnO₂ composite electrode

Firstly, pomelo peel as purchased was washed with deionized water and cut into cubes of about 2 cm×2 cm×2 cm. These cubes were put into teflon-lined reactor and hydrothermally treated at 180°C for 12 h. The processed cubes were fully washed with 50% ethanol solution and frozen in the refrigerator at -15°C for 12 h. Then the frozen pomelo

peel cubes were freeze-dried using freeze dryer under -35°C for 50 h. Finally, lyophilized cubes were carbonized in tube furnace at 800°C (heating rate: 5°C·min⁻¹) for 1 h under nitrogen protection to obtain biomass carbon aerogel. The preparation process is shown in Fig. 1.

4 g powdered PCA, 0.5 g carbon black and 0.5 g polyvinylidene fluoride were added into 40 mL of *N,N*-dimethylacetamide and mixed well. The mixture was uniformly sprayed on a 6 cm×8 cm×0.8 cm graphite plate placed on a heating board by a Hansa Infinity CRplus 0.2 mm spray gun. The graphite plate after being spraying was dried at 80°C for 12 h and then dried in vacuum drying oven at 80°C for 2 h to further remove volatile organic compounds. The load of electrode was calculated according to the weight change of graphite plate before and after being sprayed.

The preparation process of PCA-MnO₂ electrode refers to the process of PCA electrode by adding different weights of MnO₂ to *N,N*-dimethylacetamide.

Structural Characterization

The surface morphology of PCA and MnO₂ was obtained by a SU-8010 scanning electron microscope (SEM, Hitachi, Japan). A X-Pert.PRO X-ray diffractometer (XRD) made by Malvern Panalytical Ltd. was used to analyze the crystal structure of PCA and MnO₂. The specific surface area of these two main components were analyzed by BET (JW-BK100B, JWGB, China) method. Functional groups of PCA were analyzed by a NEXUS Fourier transform infrared spectrometer (FTIR).

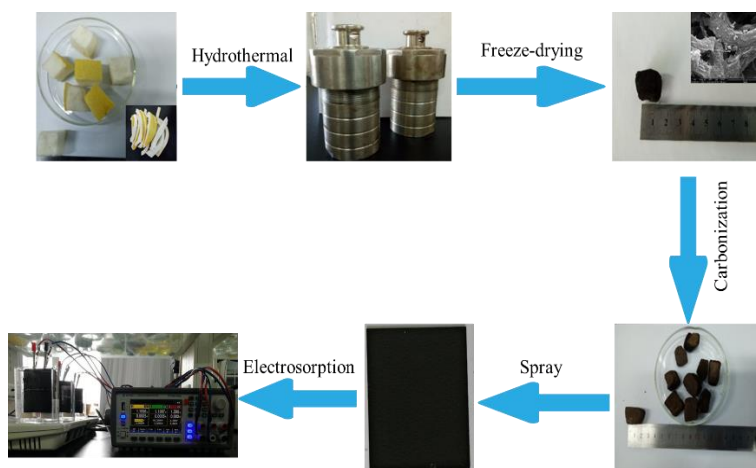


Fig. 1: Schematic representation of the preparation and electrosorption of PCA-MnO₂ composite electrode.

Electrosorption experiments

The eletrosorption device is composed of stabilized DC power, cubic organic glass tank, magnetic stirrer and electrode. The electrode distance was maintained at 6 mm. And the electrode voltage was set to 1.2 V. In order to reduce diffusion resistance of ions in solution and sampling error, the solution was stirred with magnetic stirrer at 700 rpm during electrosorption process. When concentration of ions in solution no longer changes, the electrosorption reaches equilibrium. Then the desorption process was completed by reversing the circuit. Based on the preliminary electrosorption experiment, the changes brought about by changing composition of electrode, voltage and coexisting ions on the electrosorption of Rb^+ and Cs^+ were studied. All the alkali and alkaline earth ions were determined by atomic absorption spectrophotometer. The adsorption capacities of Rb^+ and Cs^+ were calculated by equation (1):

$$q_t = \frac{(C_0 - C_t)V}{m} \quad (1)$$

where q_t is the adsorption amount at time t (h), C_0 and C_t are concentrations of initial and at contact time t respectively, V (L) is solution volume, m (g) is the mass of coating on the electrode.

Results and discussion

Electrode characterization

The key point to design an efficient electrosorption system is to prepare electrodes with large adsorption capacity. Good conductivity and large specific surface area are preconditions for large electrosorption capacity [17]. SEM images were obtained for analyzing surface morphology of materials, and studying the distribution of pores exposed on the outer surface which also is an important factor affecting the adsorption rate and amount (Fig. 2) [18]. Fig. 2a and 2b with different magnifications show that the surface of PCA is smooth with irregular shape and large internal voids which provides a large number of adsorption sites for the adsorption of ions and small diffusion resistance. In contrast, MnO_2 are submicron irregular particles with large surface area (Fig. 2c and 2d). PCA and MnO_2 are physically mixed to maintain their original morphologies respectively (Fig. 2e and 2f).

The XRD spectra of PCA and MnO_2 are shown in Fig. 3. PCA shows two broad diffraction peaks at 23° and 45° , which belongs to (002) and

(100) reflections of crystalline carbon, respectively. The broader diffraction peaks indicate that PCA has amorphous structure with a certain graphitization that makes it conductive well. Five diffraction peaks at 22.4° , 37.2° , 42.6° , 56.6° and 66.7° belong to (002), (100), (101), (102), (110) reflections of crystalline MnO_2 respectively. Compared with standard cards, it is confirmed that MnO_2 added into electrode is hexagonal $\epsilon\text{-MnO}_2$.

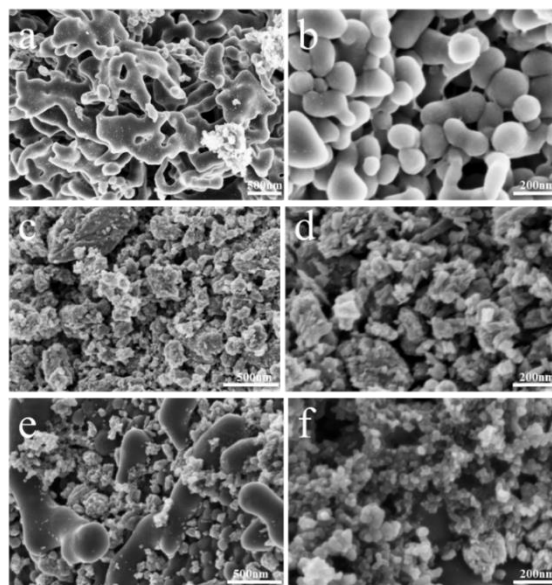


Fig. 2: SEM images of PCA (a,b), MnO_2 (c,d) and PCA- MnO_2 (e,f) electrode.

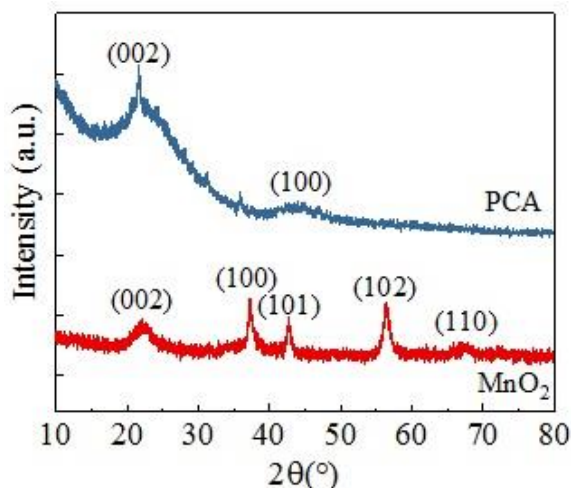


Fig. 3: XRD pattern of PCA and MnO_2 .

Porous structure in electrode materials can provide large specific surface area and a large number of adsorption sites, which is the prerequisite

for realizing high adsorption capacity in electrosorption. Based on the N_2 adsorption-desorption isotherm curve in Fig. 4, the specific surface areas of PCA and MnO_2 are calculated by BET and BJH method listed in Table 1. The specific surface area of PCA after carbonization at $800^\circ C$ is $310\text{ m}^2/g$ with pore volume of $0.255\text{ cm}^3/g$. The adsorption-desorption isotherm of PCA belongs to the fourth type of adsorption-desorption isotherm specified by IUPAC, which is the adsorption-desorption characteristic of mesoporous materials [19]. But the specific surface area of MnO_2 is only $30.3\text{ m}^2/g$ with pore volume of $0.049\text{ cm}^3/g$, which are smaller than that of PCA. These results are consistent with the situation observed in SEM images.

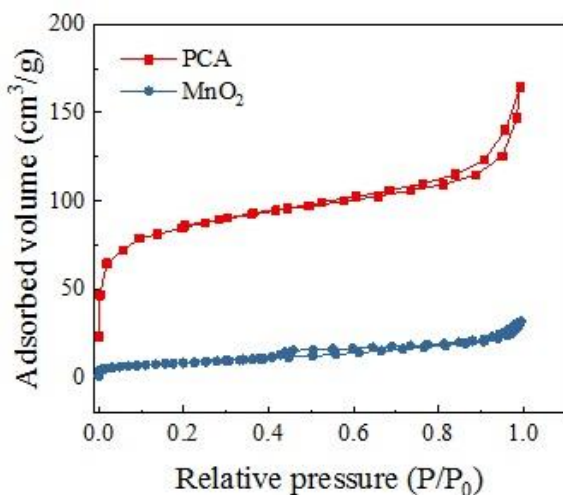


Fig. 4: Nitrogen adsorption-desorption isotherms of PCA and MnO_2 .

Table-1: Specific surface area and pore volume of PCA and MnO_2 .

Sample	Specific surface area (m^2/g)	Pore volume (cm^3/g)
PCA	310	0.255
MnO_2	30.3	0.049

The types of surface functional groups of PCA were studied by FTIR. According to FTIR spectrum in Fig. 5, the peak at 870 cm^{-1} is attributed to the stretching vibration of C-H. The peak at 1581 cm^{-1} is from the stretching vibration of C=O in the lignin. The peak at 1137 cm^{-1} refers to the asymmetric stretching of -COC-. And the peak at 3413 cm^{-1} represents the axial deformation of O-H [20]. These data indicate that part of carboxyl and hydroxyl groups still remain on the surface of PCA after high-temperature carbonization, which play important roles in metal ions adsorption.

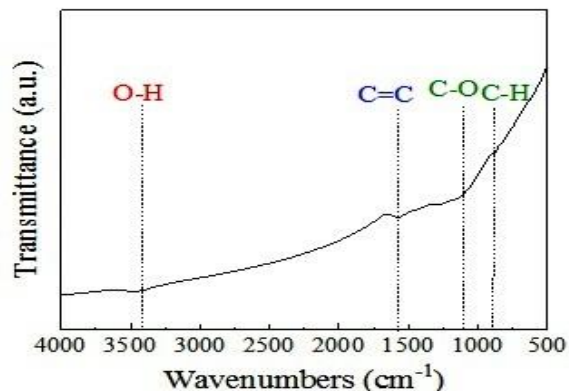


Fig. 5: FTIR spectrum of PCA.

Electrosorption of Rb^+ and Cs^+ by PCA electrode

Static electrosorption of $100\text{ mL } 2\text{ mmol/L}$ $RbCl$ and $CsCl$ was performed by PCA electrode with electrode distance of 6 mm and voltage of 1.2 V . Fig. 6 shows the effect of time on the electrosorption of Rb^+ and Cs^+ by PCA electrode. In the initial stage of electrosorption, there are large number of adsorption vacancies to ensure the rapid increase of adsorption amount. As the electrosorption process continues, the adsorption amount increased rapidly, resulting in most sites being occupied [21]. The electrosorption processes reach equilibrium after 2h, and the equilibrium adsorption capacity of PCA electrode for Rb and Cs are $12.8\text{ }\mu\text{mol/g}$ and $29.7\text{ }\mu\text{mol/g}$, respectively, which are lower than the adsorption amount of other kinds of Rb and Cs adsorbent. For example, the maximum adsorption capacity of polyacrylic acid adsorbent for Rb and Cs reached 2.0 mmol/g and 1.7 mmol/g [22]. Therefore, it is necessary to optimize the electrode and electrosorption conditions to improve its electrosorption performance of Rb and Cs .

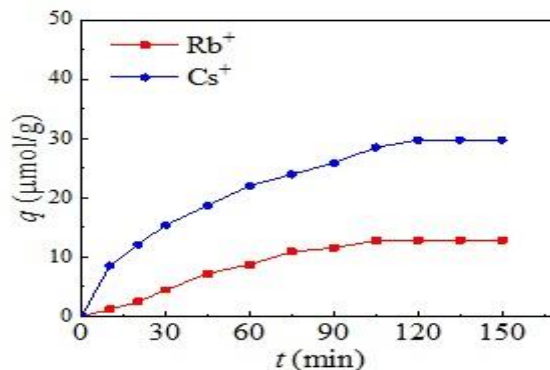


Fig. 6: Effect of time on the electrosorption of Rb^+ and Cs^+ by PCA electrode.

Electrosorption of Rb^+ and Cs^+ by PCA-MnO₂ electrode

MnO₂ is an efficient inorganic adsorbent for heavy metal ions such as Pb²⁺ and Cr³⁺ [23, 24]. However, it cannot be used alone as electrode material for electrosorption because of its non-conductive property. We combined it with PCA to prepare PCA-MnO₂ composite electrode, and studied the enhancement of Rb and Cs electrosorption.

(1) Electrosorption of Rb

The electrosorption conditions of PCA-MnO₂ composite electrode are consistent with these of PCA electrode. It can be seen from Fig. 7 that the addition of MnO₂ significantly improved the electrosorption effect of Rb⁺ on PCA-MnO₂ electrode. When the mass ratio of PCA and MnO₂ is 1:4, the equilibrium electrosorption capacity reaches a maximum of 85.4 μmol/g. But the electrosorption amount decreased as the content of MnO₂ continues to increase. The increasing amount of MnO₂ may reduce the conductivity of the PCA-MnO₂ electrode, which resulted in the poor performance of electrosorption [25-27].

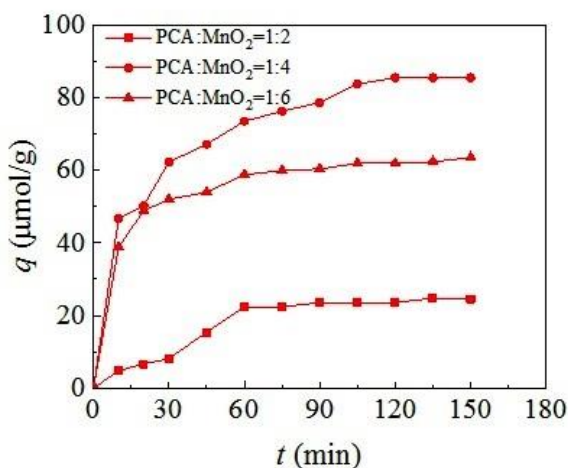


Fig. 7: Effect of time on the electrosorption of Rb⁺ by PCA-MnO₂ composite electrode.

(2) Electrosorption of Cs

Fig. 8 shows the effect of time on the electrosorption of Cs⁺ by PCA-MnO₂ electrode with different compositions under the same experimental conditions. Compared with Rb⁺, the effect of electrode composition on Cs⁺ adsorption shows the same regulation. PCA-MnO₂ (1:4) composite electrode has the largest adsorption capacity for Cs⁺, which reaches 63.8 μmol/g. But the electrosorption

amount of Cs⁺ by PCA-MnO₂ are all smaller than Rb⁺. It is attributed to the higher selectivity of MnO₂ to Rb⁺ than to Cs⁺ [28].

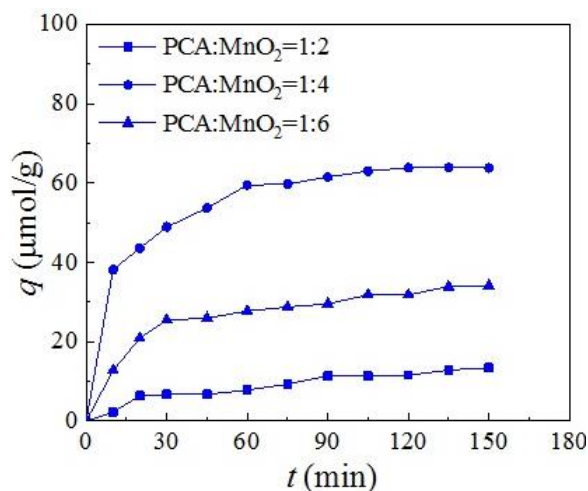


Fig. 8: Effect of time on the electrosorption of Cs⁺ by PCA-MnO₂ composite electrode.

(3) Competitive electrosorption of Rb and Cs

Rb and Cs often coexist in natural solid and liquid mineral resources due to their very similar chemical properties. When Rb⁺ and Cs⁺ are separated from solution by electrosorption method, they will inevitably affect each other during separation process. Hence the electrosorption selectivity of PCA-MnO₂ electrode for Rb⁺ and Cs⁺ in 100 mL of 1 mmol/L RbCl + 1 mmol/L CsCl solution was further studied. The effect of electrode voltage on the electrosorption selectivity in the two-component solution was also investigated. As shown in Fig. 9, the electrosorption amounts of Rb⁺ are still larger than that of Cs⁺ in the competitive system. But both of them are smaller than their respective electrosorption amounts in one-component system. When voltage is 0.8 V, the electrode has the highest electrosorption selectivity of Rb⁺ and Cs⁺. The electrosorption amount ratio of Rb⁺ and Cs⁺ reaches 8.4:1. The increase of electrode voltage devotes to increase electrosorption amounts of Rb⁺ and Cs⁺ [27, 29]. However, the electrosorption selectivity decreases during this process, which indicates that high voltage would inhibit the selectivity of the electrode for Rb⁺ and Cs⁺ [30].

Effect of alkali and alkaline earth metal ions

Natural water bodies usually dissolve other inorganic ions of different concentrations, such as Na⁺, K⁺, Mg²⁺ and Ca²⁺. Therefore, the

electrosorption of Rb^+ and Cs^+ is mainly affected by the existence of these cations with high concentration. The similar chemical properties make alkali and alkaline earth metal ions the main interference factor to the electrosorption of Rb^+ and Cs^+ . Hence, the effects of alkali/alkaline earth metal ions on the electrosorption of Rb^+ and Cs^+ on the PCA- MnO_2 electrode were investigated in stages.

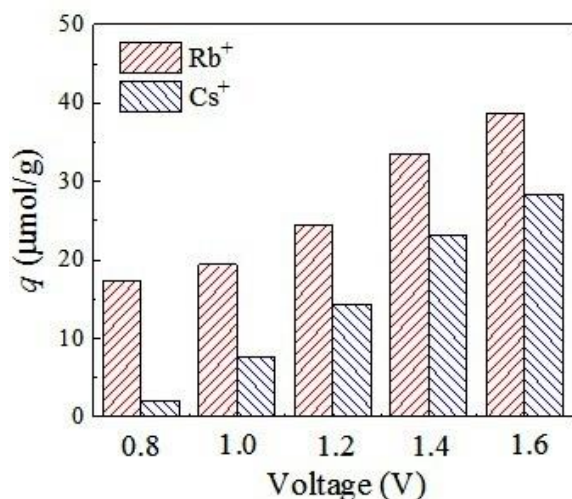


Fig. 9: Effect of electrode voltage on adsorption capacities of Rb^+ and Cs^+ .

(1) Competitive adsorption of K^+ , Rb^+ and Cs^+

Chemical properties of K^+ is very similar to Rb^+ and Cs^+ . Thus, a three-component solution of 0.5 mmol/L KCl +0.5 mmol/L RbCl +0.5 mmol/L CsCl was used to investigate the effect of coexisting K^+ on the electrosorption property of PCA- MnO_2 electrodes. Fig. 10 shows the electrosorption amounts of three kinds of ions by PCA- MnO_2 electrodes with different compositions. These electrodes have the same electrosorption selectivity order for the three ions (q : $\text{K}^+ > \text{Rb}^+ > \text{Cs}^+$). PCA- MnO_2 (1:4) composite electrode has the largest electrosorption capacity for K^+ , Rb^+ and Cs^+ , which reaches 18.4 $\mu\text{mol/g}$, 13.2 $\mu\text{mol/g}$ and 8.9 $\mu\text{mol/g}$, respectively. The electrosorption capacities of cations are related to radius of hydrated ions, specific surface area and pore size of electrode. In one-component solution, electrosorption capacity decreases with the increasing of ion hydration radius [31]. It is consistent with one-component electrosorption of PCA and PCA- MnO_2 electrodes. However, the electrosorption selectivity of the PCA- MnO_2 electrode in three-component solution is opposite to ion hydration radius.

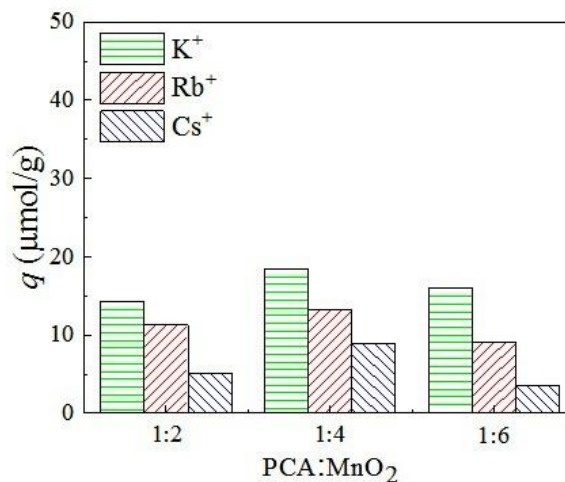


Fig. 10: Effect of coexisting K^+ on adsorption of Rb^+ and Cs^+ by PCA- MnO_2 composite electrode.

(2) Competitive electrosorption of alkali metal ions

The initial concentration of five alkali metal ions were all controlled at 0.5 mmol/L. The results of competitive electrosorption shown in Fig. 11 indicate that there is a large difference in the electrosorption selectivity of the three composite electrodes for alkali metal ions. The electrosorption amounts of alkali ions decrease with the increase of ion radius when PCA- MnO_2 (1:4) electrode is used to adsorb the five ions. These three kinds of composite electrode hardly adsorb Cs^+ under present conditions. It can be seen that composition of solution also has a significant effect on the electrosorption process of alkali metal ions.

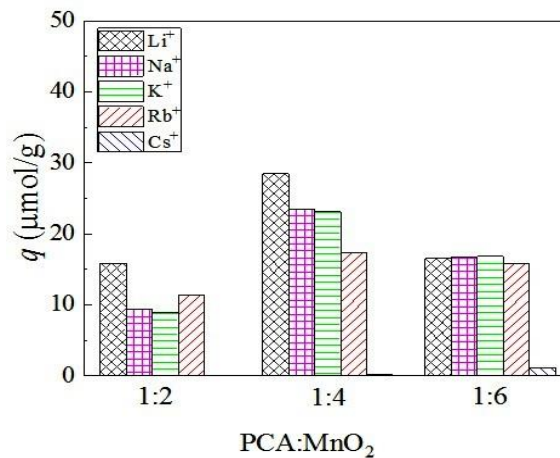


Fig. 11: Effect of coexisting alkali metal ions on adsorption of Rb^+ and Cs^+ by PCA- MnO_2 composite electrode.

Competitive electrosorption of multiple alkali/alkaline earth metal ions

When eight components of LiCl, NaCl, KCl, RbCl, CsCl, MgCl₂, CaCl₂ and SrCl₂ coexist, the three electrodes exhibit completely different electrosorption performance for the eight kinds of ions (Fig. 12). But there is an obvious phenomenon that all of the three PCA-MnO₂ electrodes have the largest electrosorption capacities for Mg²⁺. Moreover, compared with the five-component solution, the electrosorption capacities of Cs⁺ in eight-component solution increase obviously.

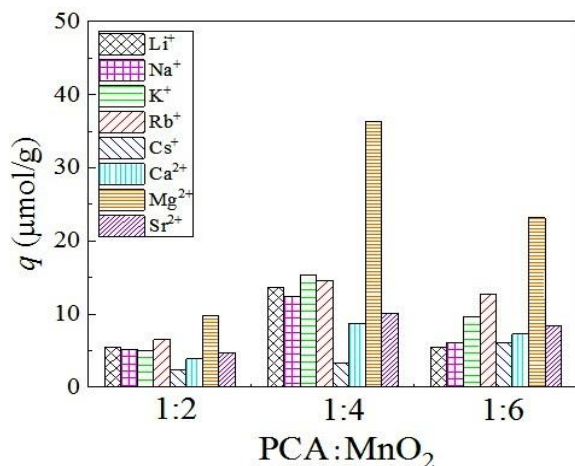


Fig. 12: Effect of coexisting alkali/alkali-earth metal ions on adsorption of Rb⁺ and Cs⁺ by PCA-MnO₂ composite electrode.

Electrosorption process involves migration of ions in solution, diffusion in the interface between electrode and solution and adsorption on the surface of electrode. Ion migration rate is affected by factors such as ion mobility and electric field intensity. The electrosorption behavior of ions in one-component solutions is affected by hydration radius, which could be affected by charge density and potential of itself [32, 33]. It makes the order of ionic radius reverse to the order of hydration radius. The hydration radius and ionic radius of the eight ions obtained from literatures are listed in Table-2. The order of ion hydration radii is Mg²⁺>Ca²⁺>Sr²⁺>Li⁺>Na⁺>K⁺>Rb⁺≈Cs⁺, while the order of ionic radius is Cs⁺>Rb⁺>K⁺>Sr²⁺>Ca²⁺>Na⁺>Li⁺>Mg²⁺. During the adsorption process of ions on the surface of electrode, ions with larger radius could occupy more surface area. When multiple metal ions coexist, ions may be adsorbed on the electrode surface after dehydrating water molecules to compete for more adsorption sites as shown in the schematic diagram (Fig. 13).

Table-2: Ionic and hydrated radii of alkali and alkaline earth metal ions.

Element	Ionic radius	Hydrated radius
Li	0.94 ^[34]	3.82 ^[34]
Na	0.95 ^[35]	3.58 ^[35]
K	1.33 ^[35]	3.31 ^[35]
Rb	1.52 ^[36]	3.29 ^[36]
Cs	1.86 ^[34]	3.29 ^[34]
Mg	0.86 ^[35]	4.28 ^[35]
Ca	0.99 ^[35]	4.12 ^[35]
Sr	1.13 ^[37]	3.90 ^[38]

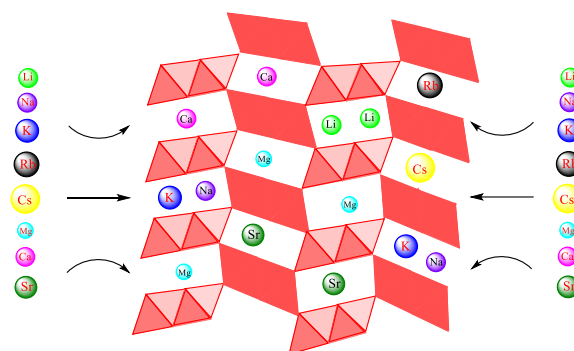


Fig. 13: Schematic diagram of electrosorption of alkali/alkali-earth metal ions by the composite electrode.

Reusability

Cyclic stability is one of the important figures of merit to evaluate the electrode performance. Good cyclic performance can reduce the cost of electrosorption process significantly. Rb⁺ was selected to investigate the cycle performance of PCA-MnO₂ (1:4) composite. After six cycles of electrosorption-desorption, the electrosorption capacity of Rb⁺ decreases from 85.4 μmol/g to 84.0 μmol/g, which confirms that the PCA-MnO₂ electrode has good cyclic electrosorption performance.

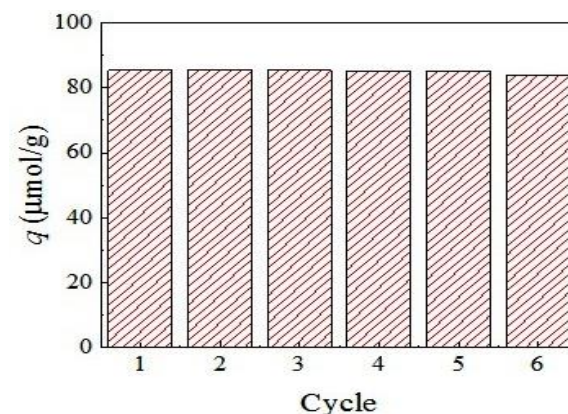


Fig. 14: Cyclic adsorption performance of Rb⁺ by PCA-MnO₂ (1:4) composite electrode.

Conclusions

In this paper, a biomass carbon aerogel with large specific surface area was prepared by hydrothermal-freeze drying-carbonization method using pomelo peel as raw material, and then sprayed onto the graphite plate to electro-adsorb Rb^+ and Cs^+ . After combining MnO_2 , the electrosorption capacities of both Rb^+ and Cs^+ increase obviously. However, too much MnO_2 may reduce the conductivity of the composite electrode, which resulted in a lower adsorption performance of electrosorption. The mass ratio of PCA and MnO_2 has a significant effect on the electrosorption selectivity of alkali and alkaline earth metal ions. When the five alkali metal ions coexist, their electrosorption capacities increase with the decrease of ion radius. After 6 electrosorption-desorption cycles, the electrosorption capacity of Rb^+ only decreases by 1.6%, which may be caused by incomplete desorption.

Acknowledgments

This work was financially supported by Joint Funds of the National Natural Science Foundation of China (U20A20150), the foundation of Qinghai Provincial Science and Technology Project, China (2018-HZ-807, 2019-ZJ-7014, 2019-ZJ-901), the Thousand Talents Plan of Qinghai province and Youth Innovative Talents Project of Department of Education of Guangdong Province (2021KQNCX026).

References

1. D. D. Qi, L. Zou and E. Hu., Electrosorption: an alternative option for desalination, *Res. J. Chem. Environ.*, **11**, 92 (2007).
2. C. C. Huang and J. C. He, Electrosorptive removal of copper ions from wastewater by using ordered mesoporous carbon electrodes, *Chem. Eng. J.*, **221**, 469 (2013).
3. Y. P. Chen, L. Peng, Q. R. Zeng, Y. Yang, M. Lei, H. J. Song, L. Y. Chai and J. D. Gu, Removal of trace Cd(II) from water with the manganese oxides/ACF composite electrode, *Clean Technol. Environ. Policy*, **17**, 49 (2015).
4. P. Xu, T. Y. Cath, A. P. Robertson, M. Reinhard, J. O. Leckie and J. E. Drewes, Critical review of desalination concentrate management, treatment and beneficial use, *Environ. Eng. Sci.*, **30**, 502 (2013).
5. C. J. Kirubakaran, D. Kalpana, Y. S. Lee, A. R. Kim, D. J. Yoo, K. S. Nahm, G. G. Kumar, Biomediated silver nanoparticles for the highly selective copper(II) ion sensor applications, *Ind. Eng. Chem. Res.*, **51**, 7441 (2012).
6. Q. L. Li, Y. J. Ding and D. X. Yuan, Electrosorption-enhanced solid-phase microextraction of trace anions using a platinum plate coated with single-walled carbon nanotubes, *Talanta*, **85**, 1148 (2011).
7. J. Zhu, H. Chen, Y. D. Wang, H. T. Guan and X. C. Xiao, Structure determination, electronic and optical properties of rubidium holmium polyphosphate $\text{RbHo}(\text{PO}_3)_4$, *J. Mol. Struct.*, **1030**, 204 (2012).
8. K. Kumar, P. Arun, C. R. Kant, N. C. Mehra and V. Mathew, The effect of cesium metal clusters on the optical properties of cesium iodide thin films, *Appl. Phys. A: Mater. Sci. Process.*, **99**, 305 (2010).
9. G. Naidu, S. Jeong, M. A. H. Johir, A. G. Fane, J. Kandasamy and S. Vigneswaran, Rubidium extraction from seawater brine by an integrated membrane distillation-selective sorption system, *Water Res.*, **123**, 321 (2017).
10. M. Onodera, A. Kirishima, S. Nagao, K. Takamiya, T. Ohtsuki, D. Akiyama and N. Sato, Desorption of radioactive cesium by seawater from the suspended particles in river water, *Chemosphere*, **185**, 806 (2017).
11. M. P. Zheng and X. F. Liu, Hydrochemistry of salt lakes of the Qinghai-Tibet plateau, China, *Aquat. Geochem.*, **15**, 293 (2009).
12. P. Y. Liu, T. T. Yan, L. Y. Shi, H. S. Park, X. C. Chen, Z. G. Zhao and D. S. Zhang, Graphene-based materials for capacitive deionization, *J. Mater. Chem. A*, **5**, 13907 (2017).
13. B. P. Jia and W. Zhang, Preparation and application of electrodes in capacitive deionization (CDI): a state-of-art review, *Nanoscale Res. Lett.*, **11**, 1 (2016).
14. Y. Liu, C. Y. Nie and X. J. Liu, Review on carbon-based composite materials for capacitive deionization, *RSC Adv.*, **5**, 15205 (2015).
15. H. J. Hong, B. G. Kim, J. Hong, J. Ryu, T. Ryu, K. S. Chung, H. Kim and I. S. Park, Enhanced Sr adsorption performance of MnO_2 -alginate beads in seawater and evaluation of its mechanism, *Chem. Eng. J.*, **319**, 163 (2017).
16. D. L. Zhao, X. Yang, H. Zhang, C. L. Chen and X. K. Wang, Effect of environmental conditions on Pb(II) adsorption on beta- MnO_2 , *Chem. Eng. J.*, **164**, 49 (2010).
17. L. J. Kong, M. H. Su, Z. H. Mai, H. P. Li, Z. H. Diao, Y. Xiong and D. Y. Chen, Removal of uranium from aqueous solution by two-dimensional electrosorption reactor, *Environ. Technol. Innovat.*, **8**, 57 (2017).
18. J. Landon, X. Gao, B. Kulengowski, J. K. Neathery and K. L. Liu, Impact of Pore Size

- Characteristics on the Electrosorption Capacity of Carbon Xerogel Electrodes for Capacitive Deionization, *J. Electrochem. Soc.*, **159**, A1861 (2012).
19. L. F. Yang and Z. Shi, Enhanced electrosorption capacity for lead ion removal with polypyrrole and air-plasma activated carbon nanotube composite electrode, *J. Appl. Polym. Sci.*, **132**, 41793 (2015).
 20. H. N. Liu, X. S. Ye, Q. Li, T. Kim, B. J. Qing, M. Guo, F. Ge, Z. J. Wu and K. Lee, Boron adsorption using a new boron-selective hybrid gel and the commercial resin D564, *Colloid. Surface. A.*, **341**, 118 (2009).
 21. R. B. Shami, V. Shojaei and H. Khoshdast, Efficient cadmium removal from aqueous solutions using a sample coal waste activated by rhamnolipid biosurfactant, *J. Environ. Manage.*, **231**, 1182 (2019).
 22. T. T. Lu, Y. F. Zhu, W. B. Wang, Y. X. Qi and A. Q. Wang, Interconnected superporous adsorbent prepared via yeast-based Pickering HIPEs for high-efficiency adsorption of Rb^+ , Cs^+ and Sr^{2+} , *Chem. Eng. J.*, **361**, 1411 (2019).
 23. H. P. Zhang, L. Q. Gu, L. Zhang, S. R. Zheng, H. Q. Wan, J. Y. Sun, D. Q. Zhu and Z. Y. Xu, Removal of aqueous $\text{Pb}(\text{II})$ by adsorption on Al_2O_3 -pillared layered MnO_2 , *Appl. Surf. Sci.*, **406**, 330 (2017).
 24. C. Luo, Z. Tian, B. Yang, L. Zhang and S. Q. Yan, Manganese dioxide/iron oxide/acid Oxidized multi-walled carbon nanotube magnetic nanocomposite for enhanced hexavalent chromium removal, *Chem. Eng. J.*, **234**, 256 (2013).
 25. F. Y. Liu, C. Z. Hu, Y. F. Li and Q. W. Liang, Preparation and Pb^{2+} electrosorption characteristics of MnO_2/CFP composite electrode, *Environ. Sci.*, **36**, 552 (2015).
 26. Y. H. Liu, T. C. Yu, Y. W. Chen and C. Y. Hou, Incorporating manganese dioxide in carbon nanotube-chitosan as a pseudocapacitive composite electrode for high-performance desalination, *ACS Sustain. Chem. Eng.*, **6**, 3196 (2018).
 27. C. Z. Hu, F. Y. Liu, H. C. Lan, H. J. Liu and J. H. Qu, Preparation of a manganese dioxide/carbon fiber electrode for electrosorptive removal of copper ions from water, *J. Colloid Interface Sci.*, **446**, 359 (2015).
 28. Z. H. Liu and K. Ooi, Preparation and alkali-metal ion extraction/insertion reactions with nanofibrous manganese oxide having 2 x 4 tunnel structure, *Chem. Mater.*, **15**, 3696 (2003).
 29. H. B. Li, S. Liang, M. M. Gao and J. Li, Uniform carbon hollow sphere for highly efficient electrosorption, *J. Porous Mat.*, **23**, 1575 (2016).
 30. Z. Huang, L. Lu, Z. X. Cai and Z. J. Ren, Individual and competitive removal of heavy metals using capacitive deionization, *J. Hazard. Mater.*, **302**, 323 (2016).
 31. X. Li, T. Close, S. Pustulka, S. Pedu, Y. Xue, C. Richter and P. Taboada-Serrano, Electrosorption of monovalent alkaline metal ions onto highly ordered mesoporous titanium dioxide nanotube electrodes, *Electrochim. Acta*, **231**, 632 (2017).
 32. Y. T. Li, T. C. Stewart and H. L. Tang, A comparative study on electrosorptive rates of metal ions in capacitive deionization, *J. Water Proc. Eng.*, **26**, 257 (2018).
 33. B. Han, B. H. He, R. Y. Geng, X. L. Zhao, P. Li, J. J. Hang and Q. H. Fan, Ni(II) sorption mechanism at the vermiculite-water interface: Effects of interlayer, *J. Mol. Liq.*, **274**, 362 (2019).
 34. S. B. Yang, N. Okada and M. Nagatsu, The highly effective removal of Cs^+ by low turbidity chitosan-grafted magnetic bentonite, *J. Hazard. Mater.*, **301**, 8 (2016).
 35. B. Tranel, J. Sager, T. Rector, J. Garland, R. F. Strayer, L. F. Levine, M. Roberts and M. Hummerick, Significance of hydrated radius and hydration shells on ionic permeability during nanofiltration in dead end and cross flow modes, *J. Bauer, Sep. Purif. Technol.*, **51**, 40 (2006).
 36. C. J. Gabelich, T. D. Tran and I. H. Suffet, Electrosorption of inorganic salts from aqueous solution using carbon aerogels, *Environ. Sci. Technol.*, **36**, 3010 (2002).
 37. H. Wang, X. L. Zhao, X. J. Han, Z. Tang, S. S. Liu, W. J. Guo, C. B. Deng, Q. W. Guo, H. H. Wang and F. C. Wu, Effects of monovalent and divalent metal cations on the aggregation and suspension of Fe_3O_4 magnetic nanoparticles in aqueous solution, *Sci. Total Environ.*, **586**, 817 (2017).
 38. A. Meleshyn, Adsorption of Sr^{2+} and Ba^{2+} at the cleaved mica-water interface: Free energy profiles and interfacial structure, *Geochim. Cosmochim. Acta*, **74**, 1485 (2010).